NANO LETTERS

Letter

pubs.acs.org/NanoLett

Molecular Motor Transport through Hollow Nanowires

Mercy Lard,*[,†] Lasse ten Siethoff,[‡] Johanna Generosi,[†,§] Alf Månsson,[‡] and Heiner Linke*[,†]

[†]Nanometer Structure Consortium (nmC@LU) and Solid State Physics, Lund University, Box 118, SE−221 00 Lund, Sweden

[‡]Department of Chemistry and Biomedical Sciences, Linnaeus University, SE-391 82 Kalmar, Sweden

[§]Nano-Science Center, Department of Chemistry, University of Copenhagen, DK-2100 Copenhagen, Denmark

Supporting Information

ABSTRACT: Biomolecular motors offer self-propelled, directed transport in designed microscale networks and can potentially replace pump-driven nanofluidics. However, in existing systems, transportation is limited to the two-dimensional plane. Here we demonstrate fully one-dimensional (1D) myosin-driven motion of fluorescent probes (actin filaments) through 80 nm wide, Al_2O_3 hollow nanowires of micrometer length. The motor-driven transport is orders of magnitude faster than would be possible by passive diffusion. The system represents a necessary element for advanced devices based on gliding assays, for example, in lab-on-a-chip systems with channel crossings and in pumpless nanosyringes. It may also serve as a scaffold for bottom-up assembly of muscle proteins into ordered contractile units, mimicking the muscle sarcomere.

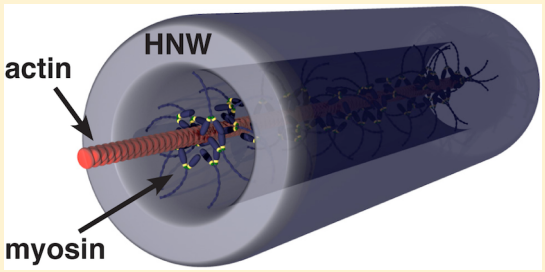

KEYWORDS: *Hollow nanowires, actin, myosin, molecular motors, motor proteins, 1D gliding assay*

The active, chemically powered transport of biomolecules by molecular motors is an attractive alternative to the use of micro- and nanofluidics for a wide range of applications. ATP-utilizing motor proteins such as kinesin or myosin can transport cytoskeletal filaments (microtubules or actin filaments, respectively) over functionalized surfaces. A significant advantage of such gliding assays compared to nanofluidics is the absence of a need for external driving forces requiring bulky accessory equipment such as pumps and control devices.[1,2]

A number of key components for controlled transport of cytoskeletal filaments have already been demonstrated, including unidirectional transport along nanofabricated, topological, or chemically defined channels,[3,4] the directed transport of analytes to detection areas,[5−7] spatiotemporal control by heating-controlled[8] or electrostatic[9] gates, automatic detection at fluorescent check points,[10] and alignment of filaments.[11,12] More advanced motor driven systems for cargo-transport[13,14] and for molecular concentration[6,7] have also been described. These developments have paved the way for a range of applications where molecular motors are combined with artificial nanostructures, for example, biosensing, e.g., in diagnostics, drug screening, and biocomputation.[5,15−18]

However, all of these hitherto demonstrated capabilities are concerned with in-plane transport and essentially two-dimensional (2D) devices. Components to introduce fully 1D transport capabilities in biomolecular, motor-driven nanodevices, such as tubes or pipes, with a diameter comparable to the size scale of the motor systems (tens of nanometers) have to date not been demonstrated. Motor-driven transport in such very thin tubes can allow transport much faster than diffusion and would enable, for example, the crossing of two transport channels by use of tunnels or bridges. This is important, for example, for error-free biocomputation[18] or the integration of 2D-nanoscale networks on multiple levels for lab-on-chip applications, and would help eliminate the need for pressure-driven fluid flow in nanosyringes[19,20] for single-cell probing or injection. Furthermore, gliding assays realized in tubes with a diameter of tens of nanometers, similar to the characteristic dimensions of the actin and myosin filament lattice in muscle, will enable controlled, fundamental studies of the 3D aspects of interactions between actin, myosin, and accessory proteins, which are thought to be critical for their function.[21]

Here we demonstrate the transport of actin filaments propelled by myosin molecular-motors through hollow nanowires (HNWs)[19] of approximately 80 nm inner diameter (Figure 1) and with a length of several micrometers. Transport of actin filaments takes place within seconds, many orders of magnitude faster than would be expected from passive diffusion, as we will show. In the following, we first demonstrate access to the inside of the HNWs (a prerequisite for functionalization) by exposing them to small Au particles (Figure 1a). We then present a device based on aligned HNWs forming a tunnel under nanofabricated Au barriers that cannot be surmounted by actin filaments (Figure 2). We will show visual evidence (Figure 3) and analysis (Figure 4) of actin filaments gliding through these HNWs underneath an Au

Received: December 19, 2013
Revised: May 23, 2014
Published: May 29, 2014

   dx.doi.org/10.1021/nl404714b | *Nano Lett.* 2014, 14, 3041−3046

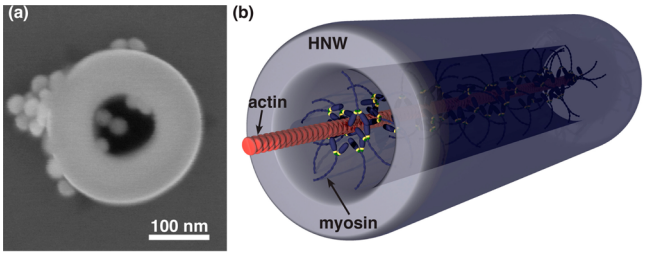

Figure 1. Scanning electron micrograph of a HNW and schematic of actomyosin in a HNW. (a) GaP nanowires from Au-particle-seeded growth on a GaP substrate are coated with 60 nm of Al_2O_3 using atomic layer deposition. The GaP core is etched away leaving behind a HNW (see Supporting Information). Au colloids, 30 nm diameter, are seen on the inside and on the outside of HNWs after overnight incubation in colloid solution and drying of the substrate. (b) Schematic of myosin binding to the inside of HNW with actin filament (diameter 10 nm) transport through the wire. The size of myosin is approximately to scale: the typical HNW inner diameter is 80 nm, and myosin molecules extend nearly 40 nm from the inner HNW surface.[22]

barrier. Finally, we discuss future applications, both for 3D control in nanotechnology and new types of fundamental studies of molecular motor systems, and show data that are strongly indicative of actin transport through HNWs positioned randomly on a flat substrate (Figure 5).

Our target device is a hollow nanowire that is functionalized, on the inside, with myosin-motor fragments (heavy meromyosin; HMM) capable of propelling actin filaments. The motor heads are known[22] to extend about 40 nm from the surface, such that a hollow nanowire with 80 nm inner diameter should, in principle, provide an optimal geometry for a 1D actomyosin gliding assay (Figure 1b).

Such hollow nanowires of controllable diameter and micrometer length can be fabricated by using epitaxially grown semiconductor nanowires (whose diameter is determined by the size of a metal seed particle), coated with a uniform oxide layer by atomic layer deposition (ALD), and with the semiconductor core subsequently removed by selective wet etching (Figure 1; see Supporting Information for details). In recent studies[23] we found that Al_2O_3 layers deposited by ALD on GaP provide for good performance (as measured by speed and fraction of motile filaments) in actomyosin gliding assays. Furthermore, the resulting Al_2O_3 can be expected to be optically transparent,[24] enabling visualization of fluorescent filaments transported through HNWs.

A prerequisite for the assembly of an in vitro motility assay (IVMA, see Supporting Information) inside a HNW is the ability to freely diffuse the components of a motility assay, including ATP, into the HNWs. We confirmed access to the inside of the HNWs by incubating them with Au particles (with 30 nm diameter). Figure 1a shows a scanning electron microscopy (SEM) image, from above, of a HNW with several colloids embedded inside, thus demonstrating that Au colloids can enter without any apparent hindrance; see Supporting Information for details. We also estimated the characteristic 1D-diffusion time over the length of 2 μm (the length scale of our HNWs) for HMM (diffusion constant $D \approx 5.9\ \mu m^2/s$; see Supporting Information) and ATP ($D \approx 300\ \mu m^2/s$) to be 0.34 s and 6.4 ms, respectively. In other words, incubation times of several seconds or more should be sufficient to enable diffusional functionalization. Factors that may further increase the required incubation time include possible crowding effects inside the HNW, as HMM begins to attach to the surface. Whereas this may not be a serious issue (due to the flexibility of the HMM[25]), we used an incubation time of 4 min to account for this (see Supporting Information for details).

A further requirement for active molecular transport inside a HNW is the maintenance, by diffusion, of adequate ATP supply, as well as ADP disposal along the length of the HNW. We do not expect this to be a limitation for our, up to 4 μm long, HNWs: based on the estimated turnover rate of ATP inside the wire and Fick's laws of diffusion, we estimate that the steady-state ATP concentration at the wire center is reduced to no less than 0.9 mM compared to 1 mM in the surrounding fluid (see Supporting Information for calculation details). Such a limited concentration reduction would have negligible effects on velocity.[26] Accumulation of ADP is another potential concern, but on the basis of similar calculations as for ATP, the maximum ADP concentration inside the wire at steady-state would be 0.08 mM. Because we neglected the additional ATP replenishing and ADP depleting effect of the creatine-kinase catalyzed reaction, the ATP and ADP concentration inside the wire would be expected to be even closer to the steady-state values in the surrounding solution (1 and 0.01 mM, respectively). Therefore, metabolic effects are expected to only minimally affect the velocity of actin filaments inside our HNWs.

In order to provide conclusive evidence of actin filaments passing through HNWs, we designed a device where HNWs form the major accessible pathway through Au barriers that cannot be readily surmounted by filaments. The overall layout of the device is shown in Figure 2. In developing this device, we first identified a suitable geometry of the Au barriers, finding that a line width of 0.7−1.0 μm and height of 200−240 nm (several times higher than the 40 nm thickness of the HMM layer[22]) effectively prevented filaments from passing above the barriers, while at the same time causing limited detachment of filaments colliding with the barrier (see Supporting Information for details). Furthermore, to achieve a high yield of HNWs exactly bridging the Au lines, we controlled the positions of HNWs using an alignment strategy:[27] electron beam lithography (EBL) was used to define wells into resist (PMMA, see Supporting Information), into which the HNWs could be brushed. After removal of the PMMA, only those HNWs that had landed in a well were left on a surface. In this way, we achieved an approximately 18% yield (HNWs in predefined wells) and 93% of those had only a single HNW bridging the Au line. As a next step, a diamond-pattern grid (diamond size: 15 μm) of 0.7 μm Au lines was aligned to the HNW pattern using EBL. The diamond shape was chosen in order to guide filaments (which tend to be propelled along walls[28]), toward the HNW entrance point, using a funnel effect (Figure 2a,b).

In Figure 2c,d we show a close-up image of a HNW embedded into an Au barrier. As one would expect, metal deposition provides a tight enclosure around the HNW, and on no occasion have we seen openings in the Au barrier next to the HNW or anywhere else, establishing that the only available transport path is in fact through the HNW.

Prior to performing motility experiments with Au barriers, we identified by SEM the coordinates of HNWs that effectively bridged Au lines (Figure 2b), and we focused our observations on these positions. Filaments were labeled with tetramethyl rhodamine iso-thiocyanate (TRITC) phalloidin (RhPh), in order to visualize transport of filaments in conjunction with the

dx.doi.org/10.1021/nl404714b | Nano Lett. 2014, 14, 3041−3046

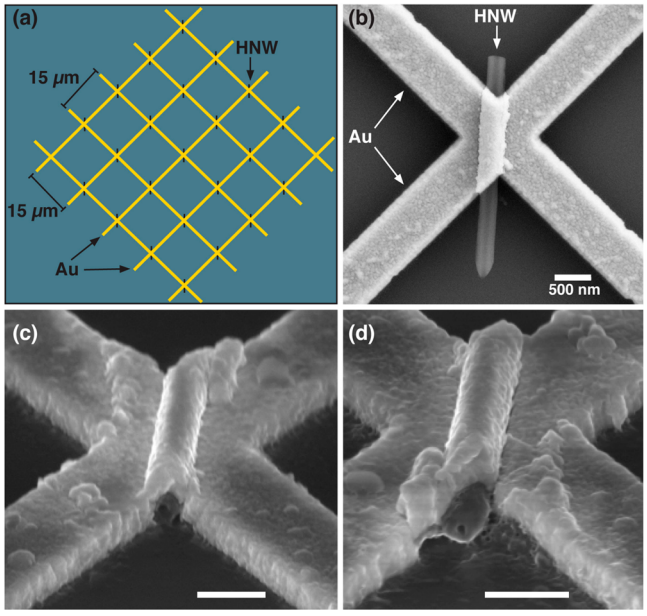

Figure 2. Schematic and scanning electron micrographs of HNW device. (a) Schematic of HNWs confined by Au diamond grid lines (0.7 μm wide and 15 μm center-to-center spacing). (b) SEM image of HNW (2.88 μm long, 80 nm inner diameter, and 200 nm outer diameter). This is the same wire as that used in Figure 3 for demonstrating transport. (c,d) Scanning electron micrographs of Au conformal coating on another HNW after use in IVMA. As shown in panel c, the HNW ends are sometimes broken off, likely during lift-off of Au. The broken ends are an advantage because they provide a direct line of access to the wires as filaments are guided to the HNW along the edges of the Au. Scale bars in panels b–d are 500 nm. Tilt in panels c and d is 52°.

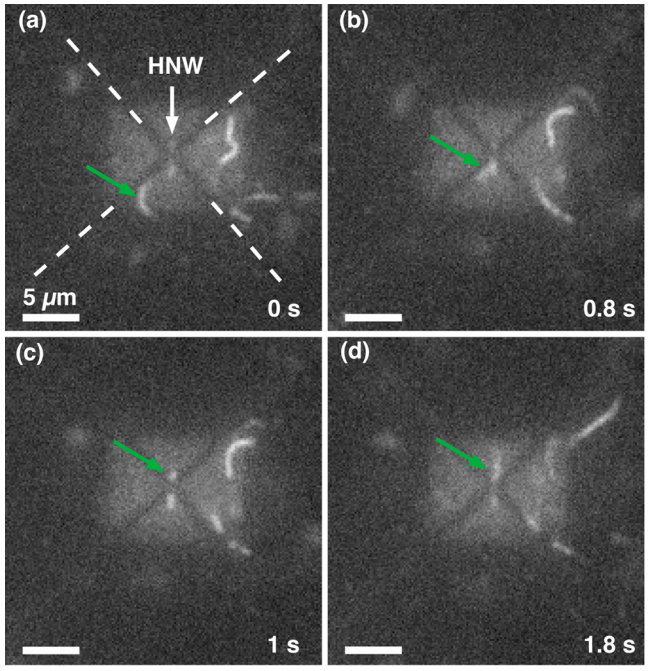

Figure 3. Motility through hollow nanowire. (a–d) Fluorescence micrographs of filament (3.14 μm long, green arrow) being transported through a HNW (see Figure 2b). Au lines are demarcated by dashed lines in panel a. Scale bar: 5 μm. The bright square region around the HNW was most likely due to carbon residues left behind during SEM imaging. We confirmed that the motility was not affected in these areas.

weakly fluorescent HNWs. Figure 3 shows a time series of fluorescence micrographs, imaged with TRITC filter set, depicting a transport event of an actin filament through a confined HNW (same wire as that in Figure 2b). Here, the filament is seen to approach the bottom end of the HNW (Figure 3a) and enter it (Figure 3b). The filament is transported through the HNW (Figure 3c) and finally exits at the top end (Figure 3d). In this experiment three HNWs were observed to transport filaments without getting blocked during the IVMA. Two other HNWs, which were capable of transport (as verified by SEM prior to IVMA) were blocked by filaments that can become stuck (immobilized) in the HNW, possibly due to dead (inactive) HMM in the HNWs that also can be typically found on flat surfaces. In order to reduce the amount of stuck filaments, it is possible to centrifuge the HMM with actin filaments in the presence of ATP, such that HMM that are inactive can be removed, prior to their use in the IVMA. Recently, drugs that can revive inactive myosin heads have been developed and can be used for reduction of inactive myosin in the IVMA.[29]

An intensity profile of the filament transported in Figure 3 can be seen in Figure 4. While the filament extends partially out from both ends of the HNW (Figure 4a), the midsection of the filament is darkened. This dark region is indicative of the filament indeed being transported through the optically transparent Al_2O_3 HNW[24] and underneath the nontransparent Au barrier. More detailed analysis confirms that the recorded image of the filament during transport is in agreement with the expected, diffraction-limited fluorescence profile of a bright object with a dark midsection (see Figure 4c, representing the actin filament with its midsection partially covered by the Au barrier, characterized by a dark gap of 1.32 μm, the width of the Au barrier). To show this, we represented the object from Figure 4b as a chain of diffraction limited point sources with the same pixel size as in Figure 4a (see Supporting Information for details). As shown in Figure 4d, the intensity profiles of the original and modeled data agree very well.

We can rule out that transport takes place over the Au barriers, based on several pieces of evidence. According to control experiments: (i) the height of the Au is sufficient to block almost all filaments from passing over the Au without detaching, temporarily, from the surface; (ii) in these controls, we saw that the few filaments that did go over barriers did not get dark and in fact were seen to become brighter and blurred (see Supporting Figure 2a), in contrast to the behavior observed in Figures 3 and 4. (iii) For HNWs, which were capable of transport, we observed that up to about four filaments passed through each HNW per minute when imaging individual HNWs for an extended time (5 min). However, when the HNWs were visibly blocked by immobile actin, transport through the barrier at these positions stopped (see Supporting Figure 2b).

In general, filaments slowed down ($p < 0.0001$; unpaired two-tailed t test) as they were transported through the HNWs. We find the speed of the filaments inside the HNWs to be approximately 2.44 ± 0.14 μm/s (mean ± standard error of the mean (SE), $n = 36$; see also Supporting Figure S1), a factor of 4 less than the speed of 9.91 ± 0.17 μm/s (mean ± SE; $n = 30$), observed for filaments moving outside the HNWs. Insight into the basis for this reduction in sliding speed will require detailed investigations that are outside the scope of the present study.

dx.doi.org/10.1021/nl404714b | Nano Lett. 2014, 14, 3041–3046

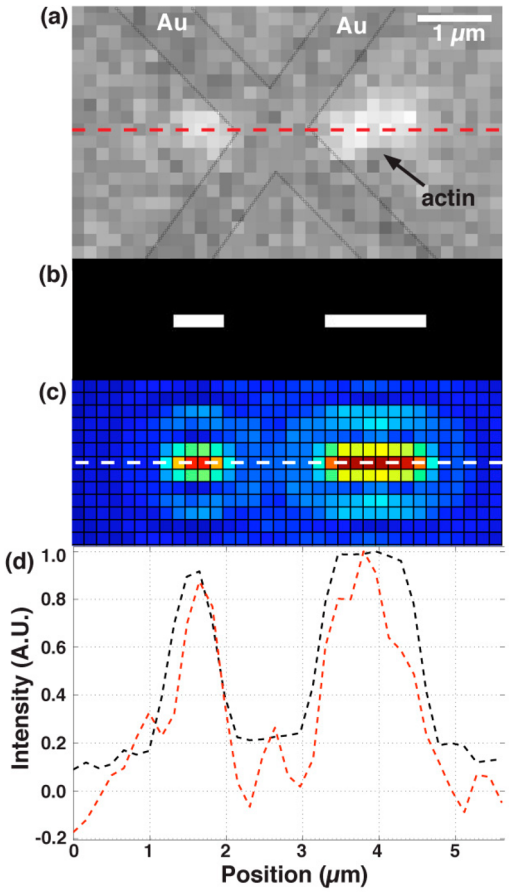

Figure 4. Analysis of filament intensity during transport. (a) Fluorescence micrograph of filament from Figure 3c. (b) Depiction of filament ends with the same lengths as visually estimated from panel a separated by a dark region with the same width as the Au barrier. (c) Sum of individual PSFs of the filament in panel b, using the same pixel size as that in panel a and treating each pixel as a point source. (d) Dashed red line: normalized intensity profile taken along the dashed red line in panel a after subtracting a background taken along the same line, 0.6 s before the filament entered the HNW. Dashed black line: normalized intensity along the center of the summed PSFs (dashed white line in panel c). See Supporting Information for details on data modeling.

Possible reasons include a low number of HMM attached inside the center of the HNW[30] and crowding effects. Alternatively, the HNWs were either slightly too narrow or too wide for optimal motor function.

For filaments that are longer than the length of the HNW, we cannot rule out that filament transport is in fact powered by myosin motors outside the HNW that push or pull the filament ends. We therefore specifically also looked for short filaments, i.e., those shorter than the length of the HNWs. Filament length was determined from intensity data.[31] Indeed, we found that filaments shorter than the HNW have similar speed (p = 0.54; two tailed, unpaired t test) as those that are longer than the HNW (Supporting Figure S1 and Supporting Movie S1). This provides further evidence of motor-powered transport inside the HNW.

Importantly, our results demonstrate that it is possible to transport fluorescent probes (actin filaments) very much faster than would be possible by diffusion. The probability that an actin filament (a thin and relatively stiff needle) would passively diffuse through a sub-100 nm tube is exceedingly small, and it would take many hours for this to happen spontaneously (see Supporting Information for details). In comparison, we observe active, molecular-motor driven transport of actin probes up to several times per minute for a given HNW. This ability opens for a range of applications in lab-on-a-chip and other nanobiotechnology areas. For example, a recent proposal for highly parallel biocomputation using self-propelled agents such as cytoskeletal filaments critically requires the ability for two pathways of actin filaments to cross, with zero probability of filaments taking a wrong turn.[18] Motor driven transport through tunnels of just a few micrometers length and less than 100 nm diameter, provides this capability. The small diameter and the geometry of the HNWs also makes them particularly suitable candidates for the development of electrostatic gating, that is, to turn on and off actin transport using an electrostatic signal, as another key element of future biocomputation or diagnostic devices. The demonstrated method is also interesting for use as nanosyringes, allowing the self-propelled, active delivery of molecules into cells,[20] without the need for pumps. For this purpose, the actin filaments could be functionalized with "load" molecules.[32]

Another exciting possible use of this system is for fundamental studies of actomyosin function. Whereas kinesin-driven microtubule transport has previously been shown in large, enclosed channels,[9] the dimensions used here are much reduced: the diameter of our HNW is comparable to the characteristic dimensions of the actin and myosin filament lattice in muscle. This opens for new types of fundamental studies of critical[21] spatial interactions between actin, myosin, and accessory proteins. Such investigations, using bottom-up assembled ordered protein arrays, would differ appreciably from studies in vivo, e.g., by allowing the use of genetically engineered proteins and a predetermined number of protein components. A range of relevant studies on other ordered actomyosin systems such as in filopodia of motile cells or other motors, i.e., the microtubule-kinesin system, may be achievable by tuning the inner diameter of the HNW.

In order to explore the possibility of myosin-driven transport through HNWs for applications where Au barriers are not required, we aimed to observe actin moving through HNWs deposited randomly onto a flat surface (that is, without the Au grid (Figure 2) used above). HNWs were transferred from the growth substrate via contact method, whereby the corner of a piece of cleanroom paper is brushed along the surface of the HNW substrate and then gently along a glass surface. Next, an IVMA with actomyosin was performed as previously stated. Filaments were labeled with Alexa Fluor 488 phalloidin (APh) and were imaged using a fluorescein isothiocyanate (FITC) microscopy filter-set (Figure 5a–c). To image the HNWs themselves, we made use of their semifluorescence when viewed using a tetramethyl rhodamine iso-thiocyanate (TRITC) filter set (Figure 5d).

On several instances, we saw actin filaments that appeared to move through HNWs (Figure 5a–c), indicated by filaments that precisely follow the path of a given HNW (imaged by TRITC filter) with single-pixel precision. However, from the images alone we cannot fully rule out that filaments perhaps moved along HNWs,[33] rather than on the inside of the optically transparent Al_2O_3 HNWs (see Supplementary Movie 2). To provide further evidence that these filaments are indeed transported inside HNWs, we make use of the fact that filaments moving through HNWs fixed under Au barriers move significantly slower than free filaments (see above). Indeed, we

dx.doi.org/10.1021/nl404714b | Nano Lett. 2014, 14, 3041–3046

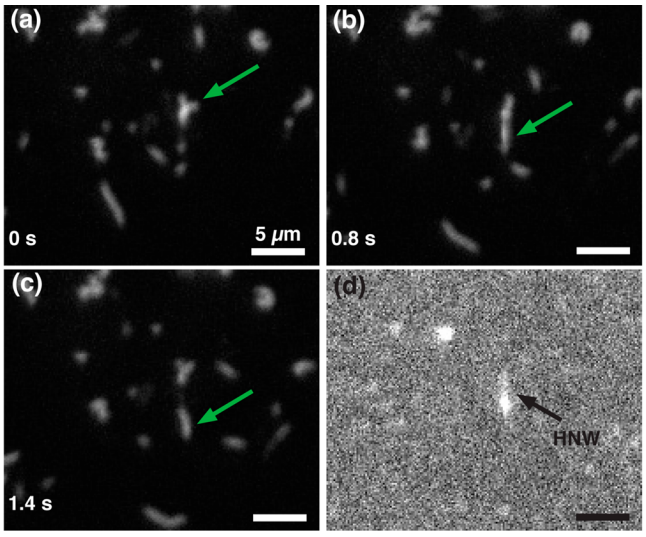

Figure 5. Motility for randomly deposited HNWs. (a) A filament (green arrow), imaged using a FITC filter set, starts at the top end of HNW, then appears to move through the HNW (b) and exits (c). Note that the Al_2O_3 HNW is expected to be optically transparent. (d) Now using a TRITC filter, the fluorescent HNW can be seen as a bright line at the same position of filament transport. The image in panel d is histogram stretched to enhance levels of brightness and contrast. Scale bar: 5 μm.

find (Supplementary Figure S3) that the average speed of the filaments appearing to move through HNWs freely deposited on a surface decreased by a factor of 2, from 5.02 ± 0.09 μm/s (mean ± SE; n = 30) observed for filaments outside HNWs in this assay, to 2.29 ± 0.21 μm/s (mean ± SE; n = 10). This statistically highly significant difference ($p < 0.0001$, two-tailed unpaired t test) accords with the idea that we observe instances of filaments moving through HNWs without the need for guiding Au barriers.

In summary, we have demonstrated the active transport of a fluorescent probe using fully 1D motor-driven transport through a narrow HNW, much faster than could be achieved by diffusion. We anticipate that the length, over which such motor-driven transport through a sub 100 nm diameter HNW can be maintained, is limited by the diffusional supply with ATP concentration to several tens of micrometers (see Supporting Information for details), a length that is fully sufficient for many applications as detailed above. Here, using a filament supply area of only 14 × 14 μm^2, we observed transport through a given HNW at several filaments per minute. This rate of transport could be substantially increased by using larger loading zones, for example, with lithographically defined regions in resist,[10] and by using tailor-made geometries for concentrating filaments,[7] as is common in devices based on gliding assays.

■ ASSOCIATED CONTENT

Ⓢ Supporting Information

Details on experimental protocols and movies of actin filament transport through HNWs. This material is available free of charge via the Internet at http://pubs.acs.org.

■ AUTHOR INFORMATION

Corresponding Authors

*(H.L.) E-mail: heiner.linke@ftf.lth.se.
*(M.L.) E-mail: mercy.lard@ftf.lth.se

Author Contributions

The manuscript was written through contributions of all authors. All authors have given approval to the final version of the manuscript.

Notes

The authors declare the following competing financial interest(s): A.M. is a co-founder, co-owner, and CEO of the start-up company ActoSense Biotech AB (Kalmar, Sweden) aiming to develop diagnostic devices based on the cytoskeletal elements, particularly actin filaments. Moreover, A.M. holds two Swedish patents and one US patent in this field, and application for one of these patents has also been filed in Europe. Finally, A.M. and L.t.S. have submitted one additional Swedish patent application with molecular motors and actin filaments in focus.

■ ACKNOWLEDGMENTS

This work was funded by the European Union Seventh Framework Programme (FP7/2007-2011) under grant agreement number 228971 (MONAD) and under grant agreement number 613044 (ABACUS), the Swedish Research Council (Projects 2010-5146 and 2010-4527), the Carl Trygger Foundation, the Crafoord Foundation, the Faculty of Natural Sciences and Engineering and the Faculty of Health and Life Sciences at Linnaeus University, the Nanometer Structure Consortium (nmC@LU), and the Knut and Alice Wallenberg Foundation.

■ REFERENCES

(1) Whitesides, G. M. *Nature* **2006**, *442* (7101), 368−373.
(2) Jokerst, J. V.; Jacobson, J. W.; Bhagwandin, B. D.; Floriano, P. N.; Christodoulides, N.; McDevitt, J. T. *Anal. Chem.* **2010**, *82* (5), 1571−1579.
(3) Sundberg, M.; Bunk, R.; Albet-Torres, N.; Kvennefors, A.; Persson, F.; Montelius, L.; Nicholls, I. A.; Ghatnekar-Nilsson, S.; Omling, P.; Tågerud, S.; Månsson, A. *Langmuir* **2006**, *22* (17), 7286−95.
(4) van den Heuvel, M. G. L.; Butcher, C. T.; Smeets, R. M. M.; Diez, S.; Dekker, C. *Nano Lett.* **2005**, *5* (6), 1117−1122.
(5) Fischer, T.; Agarwal, A.; Hess, H. *Nat. Nanotechnol.* **2009**, *4* (3), 162−166.
(6) Lin, C. T.; Kao, M. T.; Kurabayashi, K.; Meyhofer, E. *Nano Lett.* **2008**, *8* (4), 1041−6.
(7) Lard, M.; ten Siethoff, L.; Kumar, S.; Persson, M.; te Kronnie, G.; Linke, H.; Månsson, A. *Biosens. Bioelectron.* **2013**, *48*, 145−152.
(8) Schroeder, V.; Korten, T.; Linke, H.; Diez, S.; Maximov, I. *Nano Lett.* **2013**, *13* (7), 3434−3438.
(9) van den Heuvel, M. G.; de Graaff, M. P.; Dekker, C. *Science* **2006**, *312* (5775), 910−914.
(10) Lard, M.; ten Siethoff, L.; Månsson, A.; Linke, H. *Sci. Rep.* **2013**, *3*, 1092.
(11) Kim, T.; Kao, M.-T.; Hasselbrink, E. F.; Meyhöfer, E. *Nano Lett.* **2006**, *7* (1), 211−217.
(12) Yuan, J.; Pillarisetti, A.; Goldman, Y. E.; Bau, H. H. *Nano Lett.* **2012**, *13* (1), 79−84.
(13) Hess, H.; Clemmens, J.; Qin, D.; Howard, J.; Vogel, V. *Nano Lett.* **2001**, *1* (5), 235−239.
(14) Månsson, A.; Sundberg, M.; Balaz, M.; Bunk, R.; Nicholls, I. A.; Omling, P.; Tågerud, S.; Montelius, L. *Biochem. Biophys. Res. Commun.* **2004**, *314* (2), 529−534.
(15) Agarwal, A.; Hess, H. *Prog. Polym. Sci.* **2010**, *35* (1−2), 252−277.
(16) Korten, T.; Månsson, A.; Diez, S. *Curr. Opin. Biotechnol.* **2010**, *21* (4), 477−488.
(17) Nicolau, D. V., Jr.; Burrage, K.; Nicolau, D. V. *Proc. SPIE* **2007**, 6416.

(18) Nicolau, D. V.; Nicolau, D. V.; Solana, G.; Hanson, K. L.; Filipponi, L.; Wang, L. S.; Lee, A. P. *Microelectron. Eng.* **2006**, *83* (4-9), 1582−1588.
(19) Persson, H.; Beech, J.; Samuelson, L.; Oredsson, S.; Prinz, C.; Tegenfeldt, J. *Nano Res.* **2012**, *5* (3), 190−198.
(20) VanDersarl, J. J.; Xu, A. M.; Melosh, N. A. *Nano Lett.* **2011**, *12* (8), 3881−3886.
(21) Steinmetz, P. R.; Kraus, J. E.; Larroux, C.; Hammel, J. U.; Amon-Hassenzahl, A.; Houliston, E.; Worheide, G.; Nickel, M.; Degnan, B. M.; Technau, U. *Nature* **2012**, *487* (7406), 231−4.
(22) Persson, M.; Albet-Torres, N.; Ionov, L.; Sundberg, M.; Hook, F.; Diez, S.; Månsson, A.; Balaz, M. *Langmuir* **2010**, *26* (12), 9927−9936.
(23) ten Siethoff, L.; Lard, M.; Generosi, J.; Andersson, H. S.; Linke, H.; Månsson, A. *Nano Lett.* **2013**, *14* (2), 737−742.
(24) Chae, S. H.; Yu, W. J.; Bae, J. J.; Duong, D. L.; Perello, D.; Jeong, H. Y.; Ta, Q. H.; Ly, T. H.; Vu, Q. A.; Yun, M.; Duan, X.; Lee, Y. H. *Nat. Mater.* **2013**, *12* (5), 403−409.
(25) Reedy, M. C.; Beall, C.; Fyrberg, E. *Nature* **1989**, *339* (6224), 481−483.
(26) Balaz, M.; Sundberg, M.; Persson, M.; Kvassman, J.; Månsson, A. *Biochemistry* **2007**, *46* (24), 7233−7251.
(27) Lim, J. K.; Lee, B. Y.; Pedano, M. L.; Senesi, A. J.; Jang, J.-W.; Shim, W.; Hong, S.; Mirkin, C. A. *Small* **2010**, *6* (16), 1736−1740.
(28) Månsson, A.; Bunk, R.; Sundberg, M.; Montelius, L. *J. Biomed. Biotechnol.* **2012**, 2012.
(29) Radke, M. B.; Taft, M. H.; Stapel, B.; Hilfiker-Kleiner, D.; Preller, M.; Manstein, D. J.; Kelly, J. *eLife* **2014**, 3.
(30) Uyeda, T. Q. P.; Kron, S. J.; Spudich, J. A. *J. Mol. Biol.* **1990**, *214* (3), 699−710.
(31) Sundberg, M.; Balaz, M.; Bunk, R.; Rosengren-Holmberg, J. P.; Montelius, L.; Nicholls, I. A.; Omling, P.; Tågerud, S.; Månsson, A. *Langmuir* **2006**, *22* (17), 7302−7312.
(32) Kumar, S.; ten Siethoff, L.; Persson, M.; Lard, M.; te Kronnie, G.; Linke, H.; Månsson, A. *PLoS One* **2012**, *7* (10), e46298.
(33) Byun, K.-E.; Heo, K.; Shim, S.; Choi, H.-J.; Hong, S. *Small* **2009**, *5* (23), 2659−2664.